

Substrate Positioning by Gln²³⁹ Stimulates Turnover in Factor Inhibiting HIF, an α KG-Dependent Hydroxylase

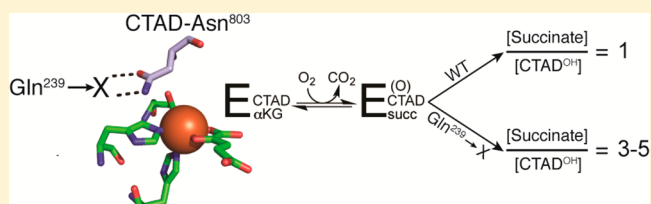
John A. Hangasky,[†] Geoffrey T. Ivison,^{†,‡} and Michael J. Knapp^{*,†}

[†]Department of Chemistry, University of Massachusetts at Amherst, Amherst, Massachusetts 01003, United States

[‡]School of Natural Science, Hampshire College, Amherst, Massachusetts 01002, United States

Supporting Information

ABSTRACT: Nonheme Fe(II)/ α KG-dependent oxygenases catalyze diverse reactions, typically inserting an O atom from O₂ into a C–H bond. Although the key to their catalytic cycle is the fact that binding and positioning of primary substrate precede O₂ activation, the means by which substrate binding stimulates turnover is not well understood. Factor Inhibiting HIF (FIH) is a Fe(II)/ α KG-dependent oxygenase that acts as a cellular oxygen sensor in humans by hydroxylating the target residue Asn⁸⁰³, found in the C-terminal transactivation domain (CTAD) of hypoxia inducible factor-1. FIH-Gln²³⁹ makes two hydrogen bonds with CTAD-Asn⁸⁰³, positioning this target residue over the Fe(II). We hypothesized the positioning of the side chain of CTAD-Asn⁸⁰³ by FIH-Gln²³⁹ was critical for stimulating O₂ activation and subsequent substrate hydroxylation. The steady-state characterization of five FIH-Gln²³⁹ variants (Ala, Asn, Glu, His, and Leu) tested the role of hydrogen bonding potential and sterics near the target residue. Each variant exhibited a 20–1200-fold decrease in k_{cat} and $k_{\text{cat}}/K_{\text{M(CTAD)}}$, but no change in $K_{\text{M(CTAD)}}$, indicating that the step after CTAD binding was affected by point mutation. Uncoupled O₂ activation was prominent in these variants, as shown by large coupling ratios ($C = [\text{succinate}]/[\text{CTAD-OH}] = 3\text{--}5$) for each of the FIH-Gln²³⁹ → X variants. The coupling ratios decreased in D₂O, indicating an isotope-sensitive inactivation for variants, not observed in the wild type. The data presented indicate that the proper positioning of CTAD-Asn⁸⁰³ by FIH-Gln²³⁹ is necessary to suppress uncoupled turnover and to support substrate hydroxylation, suggesting substrate positioning may be crucial for directing O₂ reactivity within the broader class of α KG hydroxylases.



Nonheme Fe(II)/ α KG-dependent oxygenases make up a large superfamily of enzymes catalyzing diverse reactions, including demethylations, hydroxylations, ring expansions, and epoxidations.^{1,2} Many of these enzymes have important functions in human health because of their role in O₂ sensing,^{3,4} DNA repair,^{5,6} histone demethylation,⁷ and RNA processing,^{8,9} making this superfamily a growing class of therapeutic targets.^{10,11} As the consensus chemical mechanism is an ordered sequential one, with O₂ reacting at the Fe prior to oxidation of the primary substrate (Scheme 1),^{12,13} identifying features of the active site by which substrate binding stimulates O₂ reactivity is crucial to understanding the chemistry of this superfamily. An ideal enzyme for interrogating these connections is Factor Inhibiting HIF (FIH), because of the extensive contacts with the primary substrate.¹⁴

Human cells sense O₂ through the hypoxia inducible factor (HIF) pathway, which is controlled by a small number of α KG oxygenases, including FIH.^{15,16} HIF is an $\alpha\beta$ dimeric transcription factor that regulates numerous genes involved in tissue development, controlling processes such as glycolysis, erythropoiesis, and angiogenesis.^{1,17–19} In the presence of O₂, FIH hydroxylates the β -carbon of HIF1 α -Asn⁸⁰³,²⁰ which is found in the C-terminal activation domain (CTAD) of HIF1 α . CTAD-Asn⁸⁰³ hydroxylation blocks recruitment of the cAMP response element-binding protein (CREBP), preventing HIF-

dependent gene transcription.^{4,21} The connection between CTAD-Asn⁸⁰³ positioning and O₂ reactivity is critical to understanding how substrate stimulates O₂ activation in this enzyme superfamily, as well as illuminating FIH's role as an O₂ sensor.

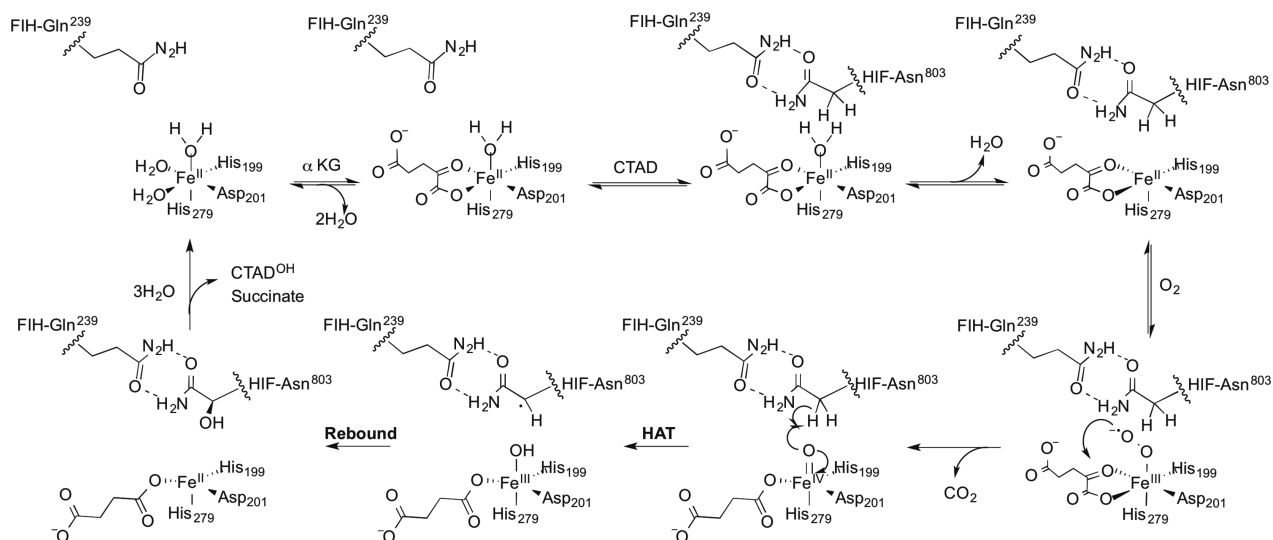
The consensus chemical mechanism for FIH is based upon an array of kinetic and spectroscopic studies of FIH and other α KG oxygenases. Kinetic studies of thymine hydroxylase, FIH, CAS, and TauD support the ordered, sequential binding of α KG and primary substrate followed by O₂.^{22–25} Although α KG, O₂, and an oxidizable compound are all substrates for these enzymes, we will refer to the oxidizable substrate as the “primary substrate”. Spectroscopic studies of CAS,^{26–28} TfdA,²⁹ FIH,³⁰ and TauD³¹ revealed that the Fe(II) released an aquo ligand after the primary substrate bound, creating a site for O₂ binding. Binding and activation of O₂ lead to the oxidative decarboxylation of α KG and the formation of a highly reactive ferryl intermediate (Scheme 1). Although the precise sequence of intermediates is not known, the ferryl intermediate has been observed in TauD^{32–34} and P4H,³⁵ demonstrating that H atom abstraction by the ferryl intermediate occurs,³⁶ with the next

Received: June 6, 2014

Revised: August 7, 2014

Published: August 13, 2014

Scheme 1. Proposed Chemical Mechanism of FIH



step likely to be $\cdot\text{OH}$ rebound to hydroxylate the primary substrate.

The most intriguing feature of the consensus mechanism is that binding the primary substrate stimulates O_2 reactivity.^{22,37,38} Loss of an aquo ligand when the primary substrate is bound opens a coordination site for O_2 binding, as observed upon binding of the primary substrate in several αKG -dependent oxygenases, including CytC3, TauD, CAS, and FIH.^{26,30,31} Although aquo release is central to the widely accepted model for substrate-stimulated O_2 activation,³⁹ we note that simple ligand exchange is insufficient for O_2 activation in these enzymes. For example, substrate binding to FIH leads to only fractional release of the aquo ligand,³⁰ and mutagenesis suggests that hydrogen bond donors to the αKG are necessary for full activity in this enzyme.⁴⁰ Computational studies^{41–44} and mechanistic probes^{45–47} further point to turnover being limited by steps after O_2 binds to the Fe(II). These and related observations lead us to propose that substrate-stimulated O_2 reactivity arises from bonding changes throughout the active site, ranging from aquo release at the iron cofactor to altered contacts in the second coordination sphere.

A focus of this research in our lab is to identify those active site features that change upon substrate binding to stimulate O_2 activation in αKG oxygenases. Although the precise sequence of intermediates formed during turnover is not known, we define O_2 activation as the steps between O_2 binding and oxidative decarboxylation (Scheme 1) by virtue of the irreversible chemistry; this step is depicted as the nucleophilic attack of the putative ferric superoxide on the α -keto position of αKG . On the basis of known crystal structures of FIH,^{14,48,49} we have used point mutagenesis to identify several essential second-coordination sphere interactions in FIH, including those hydrogen bonding to Fe(II) ligands, as well as FIH-Gln²³⁹, an anchor residue that forms two hydrogen bonds with the target residue, CTAD-Asn⁸⁰³ (Figure 1).¹⁴ Intriguingly, disruption of this two-point hydrogen bond in the FIH-Gln²³⁹ \rightarrow Asn point mutant led to a decrease in k_{cat} of 250-fold, but a negligible change in $K_{\text{M(CTAD)}}$.⁴⁰ This was attributed to a combination of steric hindrance near the open coordination site on Fe(II) and incorrect CTAD positioning for the HAT step. Subsequently, it was shown that an irreversible step associated with O_2 activation was rate-limiting in wild-type FIH (WT-

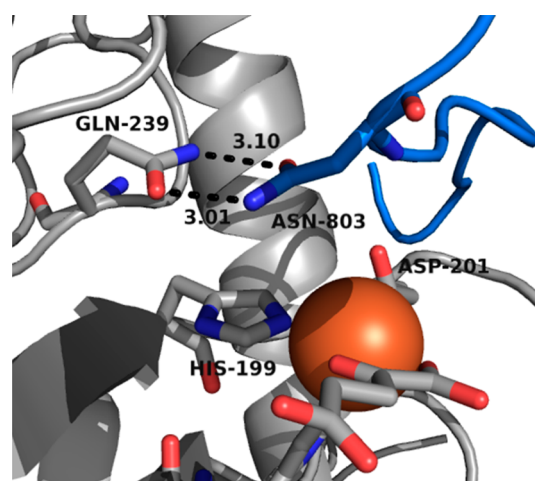


Figure 1. CTAD-Asn⁸⁰³ (CTAD, blue) positioned by FIH-Gln²³⁹ (FIH, gray) over the active site. Hydrogen bonding distances are given in angstroms (Protein Data Bank entry 1H2L¹⁴).

FIH),²⁵ suggesting that the slower turnover for the Gln²³⁹ \rightarrow Asn variant could arise from slower O_2 activation. This suggests the intriguing possibility that target residue position may stimulate O_2 activation and that the overall structure of the active site is crucial for O_2 activation.

This study tests the role of Gln²³⁹ in substrate hydroxylation in αKG oxygenases. As FIH hydroxylates a specific target residue within a large peptide (CTAD-Asn⁸⁰³), our focus was directed at this target residue pocket, formed by the side chains of FIH residues Tyr¹⁰², His¹⁹⁹, Arg²³⁸, and Gln²³⁹ (Figure 1). Five FIH-Gln²³⁹ \rightarrow X variants were prepared (X = Ala, Asn, Glu, His, and Leu) to vary the bulk and hydrogen bonding potential within the target residue pocket. Although these variants exhibited significantly reduced steady-state rate constants that decreased monotonically with increasing residue bulk, CTAD binding affinity was unaffected by mutation. In contrast to the case in WT-FIH, O_2 activation was appreciably uncoupled from CTAD hydroxylation in the variants; uncoupled O_2 activation was partially suppressed in D_2O . These data establish that the proper orientation of CTAD-Asn⁸⁰³ by FIH-Gln²³⁹ is required for substrate hydroxylation,

most likely because of the need for the proper target residue positioning during steps after O₂ activation.

■ EXPERIMENTAL PROCEDURES

Materials. All reagents were purchased from commercial vendors and were not further purified, with the exception of the 39-mer CTAD peptide. The 39-mer CTAD peptide corresponding to the C-terminal activation domain of human HIF1 α , (HIF1 α ^{788–826}) contained a Cys⁸⁰⁰ → Ala change (underlined) (DEGLPQLTSYDAEVNAPIQGSRNLLQGEE-LLRALDQVN). This was purchased as a desalted peptide from EZBiolab (Carmel, IN) with free N- and C-termini. The peptide was purified as previously described using reverse-phase high-performance liquid chromatography (RP-HPLC) to obtain >95% pure CTAD.²⁵ The 19-mer CTAD peptide corresponding to HIF1 α ^{788–806} also contained a Cys⁸⁰⁰ → Ala change and was purchased at >95% purity from EZBiolab with free N- and C-termini. The CTAD-Asn⁸⁰³ → Gln peptide was the 19-mer sequence but contained the Asn⁸⁰³ → Gln change (DEGLPQLTSYDAEVQAPI).

FIH Mutations. The Stratagene QuikChange mutagenesis kit was used to introduce the mutations into the pET28a-FIH construct.⁵⁰ All mutations were sequenced (Genewiz) to confirm that the DNA sequence contained only the desired point mutation. Sequenced plasmids were transformed into BL21(DE3) cells for protein expression.

Protein Expression and Purification. WT-FIH and all variants were overexpressed in *Escherichia coli* with an N-terminal His₆ tag and purified as previously described.²⁵ Three additional residues (NH₂-GlySerHis-) from the fusion protein remained on the N-terminus following thrombin cleavage. Purified FIH was buffer-exchanged into 50 mM HEPES (pH 7.00). The purity (>95%) of each variant was assessed by sodium dodecyl sulfate–polyacrylamide gel electrophoresis.

Steady-State Kinetics Assays. All assays used saturating concentrations of FeSO₄ (25 μ M) and ascorbate (2 mM) and an ambient O₂ concentration (217 μ M at 37.0 °C) and were performed in 50 mM HEPES (pH 7.00) at 37.0 °C unless specifically noted otherwise. DTT (200 μ M) was added to assays for FIH-Gln²³⁹ → His and FIH-Gln²³⁹ → Glu when these variants were tested in D₂O, as nonlinear progress curves were observed otherwise. Assays in which CTAD was the varied substrate (from 15 to 300 μ M) utilized a saturating α KG concentration (500 μ M). Assays with α KG as the varied substrate (from 2.5 to 100 μ M) utilized a fixed CTAD concentration of 100 μ M [$\sim K_{M(CTAD)}$] to conserve on the use of the peptide. Assay reagents were mixed and incubated for 2 min at 37.0 °C before the addition of enzyme ($[E]_T = 1.5–10$ μ M). Reaction aliquots (5 μ L) were quenched with a 75% acetonitrile/0.2% TFA mixture (20 μ L) saturated with 3,5-dimethoxy-4-hydroxycinnamic acid and analyzed for peptide hydroxylation using a Bruker Daltonics Omnisflex matrix-assisted laser desorption ionization time-of-flight mass spectrometry (MALDI-TOF MS) instrument. Initial rates were determined from five to seven quenched time points (0 to \sim 15% fractional conversion). The nonlinear least-squares fitting of initial rate data to the Michaelis–Menten equation yielded the apparent steady-state rate constants, k_{cat} and k_{cat}/K_M . All assays were replicated a minimum of three times.

Solvent Kinetic Isotope Effects (SKIEs). Steady-state assays for SKIEs were performed under the same conditions reported above, with the exception that all reagents were prepared in D₂O. Deuterium oxide (D, 99.9%) was purchased

from Cambridge Isotope Laboratories (Andover, MA) and used as received. Working FIH stock solutions were made by diluting high-concentration stocks from H₂O into D₂O containing 50 mM HEPES (pD 7.00). Assays were performed in 50 mM HEPES (pD 7.00), with a final D₂O percentage estimated to be 96%. SKIEs were calculated from the direct comparison of kinetic parameters observed in buffers containing H₂O and D₂O; e.g., $^{D_2O}k_{cat} = k_{cat(H_2O)}/k_{cat(D_2O)}$.

Succinate Quantification. The coupling between the two half-reactions was determined by monitoring the production of succinate and CTAD^{OH} concentrations in several quench points from a common reaction. Reactions of α KG (500 μ M), FeSO₄ (25 μ M), CTAD (350 μ M), and FIH (5–10 μ M) were conducted at 37.0 °C and analyzed similarly using previously reported procedures.^{25,40,47} As HEPES interfered with the succinate analysis, the reaction buffer consisted of 50 mM Tris (pL 7.00). A Hamilton PRP-X300 anion exclusion column was used to separate the succinate produced from the quenched reactions, and UV detection at 210 nm was used to determine the succinate concentration. Using aliquots from the same quenched assay, a Bruker Daltonics Omnisflex MALDI-TOF MS was used to determine the CTAD^{OH} concentration. The coupling ratio (*C*) was determined by taking the ratio of the rate of succinate formation and the rate of CTAD^{OH} formation from matched time points.

Fluorescence Spectroscopy. The FIH–CTAD binding constants were measured through quenching of the intrinsic tryptophan fluorescence of (Co + α KG)FIH upon CTAD binding at room temperature (\sim 20 °C). The fluorescence cuvette contained FIH (1.5 μ M), CoSO₄ (25 μ M), α KG (500 μ M), and 50 mM HEPES (pH 7.05). This solution was titrated with 50 mM HEPES (pH 7.05) containing CTAD (1 mM), FIH (1.5 μ M), CoSO₄ (25 μ M), and α KG (500 μ M). All titrations were performed aerobically. After each addition of titrant, samples were gently mixed and allowed to equilibrate for 5 min before being excited at 295 nm. The fluorescence intensities at 330 nm were plotted versus the total CTAD concentration and fit using eq 1

$$\frac{I - I_0}{I_f - I_0} = \frac{[E] + [S] + K_D - \sqrt{([E] + [S] + K_D)^2 - 4[E][S]n}}{2[E]} \quad (1)$$

where *I* is the measured fluorescence intensity, [E] is the protein concentration, [S] is the total CTAD concentration, *n* is the number of binding sites, and *K_D* is the binding affinity. The initial intensity (*I*₀) and final intensity (*I*_f) were obtained from measured spectra.

■ RESULTS

Variants of FIH-Gln²³⁹ were used to test the effect of target residue positioning on substrate hydroxylation in FIH. The variants were designed to vary hydrogen bonding potential (Gln²³⁹ → Glu and Gln²³⁹ → His) and cavity size (Gln²³⁹ → Ala, Gln²³⁹ → Asn, and Gln²³⁹ → Leu) in the target residue pocket of FIH. The Gln²³⁹ variants were kinetically characterized in the steady state with CTAD as the varied substrate, giving the apparent rate constants k_{cat} and $k_{cat}/K_{M(CTAD)}$. The kinetic characterization revealed significantly diminished rate constants for turnover, leading us to determine

the binding affinity of CTAD as well as the coupling ratio of the two half-reactions for each point mutant.

Kinetic Characterization of Gln²³⁹ → X Variants. We hypothesized the positioning of CTAD-Asn⁸⁰³ by FIH-Gln²³⁹ was necessary to support turnover and therefore focused our studies on steady-state characterization by monitoring CTAD^{OH} formation via MALDI-TOF. Although O₂ uptake was the first method that we considered, the slow turnover for FIH makes high-precision kinetic determinations by this method challenging. Assays using fixed concentrations of αKG (500 μM) and O₂ (217 μM) and varied concentrations of CTAD (15–300 μM) were used to measure initial rates, which were then fit to the Michaelis–Menten equation to obtain the apparent steady-state rate constants, k_{cat} and $k_{\text{cat}}/K_{\text{M(CTAD)}}$. The Michaelis constant for αKG was determined for each variant [$K_{\text{M(αKG)}} = 4\text{--}7\ \mu\text{M}$], which was slightly lower than that for WT-FIH [$K_{\text{M(αKG)}} = 16\ \mu\text{M}$]. Because of the O₂ concentration is subsaturating, the apparent k_{cat} encompasses all steps after CTAD binding, including those involved in O₂ binding and activation. All of the Gln²³⁹ → X variants exhibited a significant decrease in k_{cat} (Figure 2). The Gln²³⁹ → Ala (k_{cat}

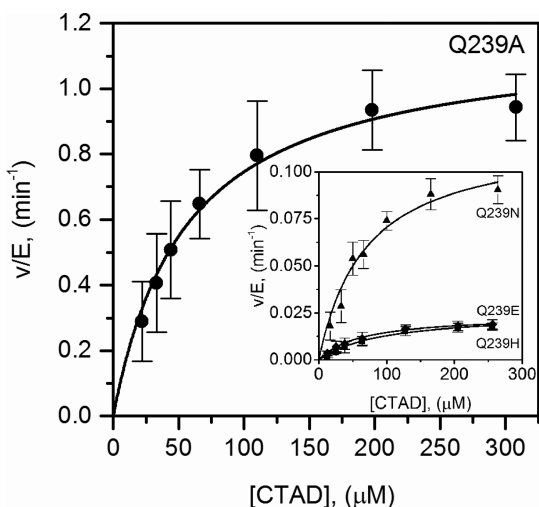


Figure 2. Steady-state kinetics of Q239A in H₂O. FIH (1.5 μM), ascorbate (2 mM), αKG (500 μM), FeSO₄ (25 μM), and CTAD (0–300 μM) were in 50 mM HEPES (pH 7.00). The inset shows the steady-state kinetics of Q239N (▲), Q239H (■), and Q239E (◆) in H₂O. FIH (1.5–30 μM), ascorbate (2 mM), αKG (500 μM), FeSO₄ (25 μM), and CTAD (0–300 μM) were in 50 mM HEPES (pH 7.00).

$= 1.27 \pm 0.10\ \text{min}^{-1}$) variant was most active, as the k_{cat} decreased 20-fold relative to that of WT-FIH, whereas the k_{cat} for Gln²³⁹ → Asn ($0.14 \pm 0.02\ \text{min}^{-1}$) decreased 200-fold. The k_{cat} for variants capable of one-point hydrogen bonding decreased >1200-fold: Gln²³⁹ → His ($0.023 \pm 0.003\ \text{min}^{-1}$) and Gln²³⁹ → Glu ($0.024 \pm 0.002\ \text{min}^{-1}$). We were unable to observe hydroxylation from the Gln²³⁹ → Leu variant.

Steps from CTAD binding through the first irreversible step (decarboxylation) comprise $k_{\text{cat}}/K_{\text{M(CTAD)}}$ (Scheme 2). The effect of each point variant on $k_{\text{cat}}/K_{\text{M(CTAD)}}$ was nearly identical to their effect on k_{cat} , indicating that the variants affected a step that was separate from CTAD binding.

We tested the activity of FIH-Gln²³⁹ → Asn using a 19-mer CTAD peptide containing the complementary CTAD-Asn⁸⁰³ → Gln point mutation, which switched the residues at this interface. This switch mutation was designed to restore the bulk

and hydrogen bonds observed between WT-FIH and WT-CTAD. However, the activity level was below our detection limit ($0.002\ \text{min}^{-1}$), as hydroxylated CTAD-Asn⁸⁰³ → Gln was not detected upon being incubated with FIH-Gln²³⁹ → Asn. WT-FIH was similarly unreactive toward this variant CTAD, as WT-FIH hydroxylated the 19-mer WT-CTAD with an appreciable rate, but did not hydroxylate the variant CTAD (Table 1).

Binding Affinity of CTAD for Gln²³⁹ → X Variants. The binding affinity of each FIH variant for CTAD was measured by titration using the intrinsic tryptophan fluorescence of FIH. A solution containing CTAD (1 mM) was titrated into a solution containing FIH (1.5 μM) while the fluorescence at 330 nm was monitored ($\lambda_{\text{ex}} = 295\ \text{nm}$); both solutions were anaerobic and contained CoSO₄ (25 μM) and αKG (500 μM). The change in fluorescence intensity (330 nm) was plotted as a function of CTAD concentration and fit to eq 1. The experimentally determined K_{D} for each point mutant (Table 2) was similar to that of WT-FIH ($78 \pm 7\ \mu\text{M}$), indicating the thermodynamics of CTAD binding was not affected by point mutation.

Uncoupled Turnover in the Gln²³⁹ → X Variants. The kinetic parameters of the Gln²³⁹ → X mutations led us to explore the coupling of O₂ activation to substrate hydroxylation. We hypothesized that if the conformational state of CTAD-Asn⁸⁰³ were incorrect for HAT, then the two half-reactions would uncouple to produce more succinate than hydroxylated product (CTAD^{OH}). Quenched aliquots from reaction mixtures containing saturating concentrations of αKG (500 μM) and CTAD (350 μM) in 50 mM Tris (pH 7.00) were analyzed for CTAD^{OH} via MALDI-TOF MS and succinate via HPLC. Tris buffer was used for these assays to minimize the background signal in the HPLC chromatograms that arose due to buffer components.

The coupling values for the Gln²³⁹ → X (X = Ala, Asn, Glu, and His) variants were obtained by taking the ratio of the rates of formation for succinate and CTAD^{OH}. Variants produced three to five succinates per equivalent of CTAD^{OH}; succinate formation was observed for the Gln²³⁹ → Leu variant [$k_{\text{obs(suc)}} = 0.08\ \text{min}^{-1}$], indicating O₂ activation occurred even though CTAD hydroxylation was not detected for this variant (Table 3). This uncoupling is similar to the values found previously for second-coordination sphere variants of FIH.⁴⁰

The coupling of WT, Gln²³⁹ → Ala, and Gln²³⁹ → Asn in deuterated buffer was used to determine if the coupling ratio changed between protonated and deuterated buffers. The coupling for WT FIH in H₂O ($C = 1.0 \pm 0.1$) and D₂O ($C = 1.0 \pm 0.1$) was in agreement with our previous work,²⁵ showing WT remains tightly coupled under all tested conditions. However, the coupling ratio in D₂O for Gln²³⁹ → Ala ($C = 1.4 \pm 0.2$) and Gln²³⁹ → Asn ($C = 2.2 \pm 0.2$) approached unity, indicating that solvent deuteration led to more tightly coupled turnover for these variants.

Solvent Kinetic Isotope Effects (SKIEs). SKIEs on both k_{cat} and $k_{\text{cat}}/K_{\text{M(CTAD)}}$ were used to test the importance of solvent-dependent steps during turnover. Initial rates from steady-state assays using saturating αKG concentrations (500 μM), ambient O₂ concentrations (217 μM), and varied concentrations of CTAD (15–300 μM) were fit to the Michaelis–Menten equation (Figure 3). Turnover was faster in D₂O with both WT-FIH and each variant, leading to an inverse SKIE on k_{cat} and $k_{\text{cat}}/K_{\text{M(CTAD)}}$ (Table 4). However, these SKIEs must be considered in the context of the solvent-dependent uncoupling observed for the variants.⁵¹

Scheme 2. Minimal Chemical Scheme for Uncoupling

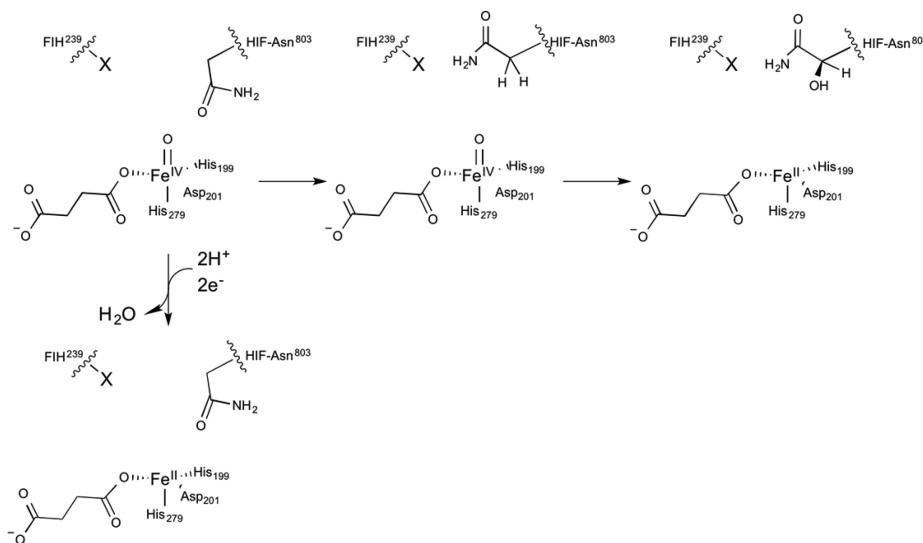


Table 1. Initial Rates for 19-mer Peptides CTAD and CTAD-N803Q^a

	initial rate (min ⁻¹)	
	WT-CTAD	CTAD-N803Q
WT	0.70	<0.005 ^b
Q239N	<0.005	<0.005 ^b

^aAssays contained ascorbate (2 mM), α KG (500 μ M), FeSO₄ (25 μ M), and 19-mer CTAD (400 μ M) in 50 mM HEPES (pH 7.00) at 37.0 °C. The CTAD peptide used contained 19 residues. ^bNo activity detected; estimated detection limit, if active.

DISCUSSION

The ordered sequential consensus mechanism for α KG oxygenases leads to coupled turnover when primary substrate binding stimulates reactivity toward O₂, a phenomenon termed substrate-induced activity enhancement,⁵² priming,⁵³ or triggering⁵⁴ by different groups. As primary substrate does not directly bind to the Fe(II), altered local contacts within the active site likely stimulate O₂ activation. Although the idea of stimulated O₂ activation refers to the empirical observation of increased turnover rates induced by substrate binding, the dominant model used to explain this focuses on aquo release, which creates an open coordination site for O₂ binding.³⁹ In our opinion, broader changes within the active site are correlated with this effect, such as the position of the primary substrate.

Table 2. Apparent Kinetic Parameters for FIH and Its Variants^a

	k_{cat} (min ⁻¹) ^b	$k_{cat}/K_M(CTAD)$ (μ M ⁻¹ min ⁻¹) ^b	$K_M(CTAD)$ (μ M) ^b	$K_D(CTAD)$ (μ M) ^c	$K_M(\alpha$ KG) (μ M) ^d
WT	30 ± 2.5 ^e	0.4 ± 0.1 ^e	70 ± 20 ^e	78 ± 7 ^f	16 ± 3.0
Q239A	1.3 ± 0.10	0.021 ± 0.002	61 ± 10	100 ± 16	5.0 ± 0.5
Q239N	0.14 ± 0.02	2.0 × 10 ⁻³ ± 8 × 10 ⁻⁴	74 ± 30	98 ± 10	4.0 ± 0.4
Q239H	0.023 ± 0.003	(3.4 ± 1) × 10 ⁻⁴	68 ± 18	64 ± 14	7.0 ± 1.4
Q239E	0.024 ± 0.002	3.4 × 10 ⁻⁴ ± 7 × 10 ⁻⁵	71 ± 10	75 ± 15	4.7 ± 2.0
Q239L	<0.005 ^g	<8 × 10 ^{-5g}	ND ^h	80 ± 8	ND ^h

^aIn 50 mM HEPES (pH 7.00) at 37.0 °C. ^bAssays in which CTAD was the varied substrate, in ascorbate (2 mM), α KG (500 μ M), FeSO₄ (25 μ M), and CTAD (0–300 μ M). ^cDetermined using intrinsic tryptophan fluorescence with Co-substituted enzyme. ^dAssays in which α KG was the varied substrate, in ascorbate (2 mM), α KG (2–200 μ M), FeSO₄ (25 μ M), and CTAD (100 μ M). ^eFrom ref 25. ^fFrom ref 30. ^gNo activity detected; estimated detection limits as reported. ^hNot determined.

Table 3. Coupling of Succinate and CTAD^{OH} Concentrations for FIH and Variants^a

	$k_{obs(H_2O)}$ ([succinate] min ⁻¹ [FIH] ⁻¹)	C_{H_2O} ^b	C_{D_2O} ^b
WT	28 ± 2	1.0 ± 0.1	1.0 ± 0.1
Q239A	5.5 ± 0.3	4 ± 1	1.4 ± 0.2
Q239N	0.49 ± 0.08	3.3 ± 0.3	2.2 ± 0.2
Q239H	0.06 ± 0.02	3 ± 1	ND ^c
Q239E	0.07 ± 0.03	5 ± 1	ND ^c
Q239L	0.08 ± 0.02	ND ^c	ND ^c

^aReaction mixtures contained FIH (5–10 μ M), α KG (500 μ M), FeSO₄ (25 μ M), and CTAD (350 μ M) in 50 mM Tris (pH 7.00) at 37 °C. ^b $C = (\text{moles of succinate per minute})/(\text{moles of CTAD}^{OH} \text{ per minute})$. ^cNot determined.

FIH is notable in that enzyme–substrate contacts are quite extensive because the substrate is a large peptide (CTAD), with the target residue positioned above the Fe by a two-point hydrogen bond to the side chain of an anchoring residue, FIH-Gln²³⁹.^{14,55} This study varied the sterics and H-bonding potential of this anchor residue to test its role in hydroxylating CTAD-Asn⁸⁰³.

CTAD Hydroxylation Is Slowed by Gln²³⁹ Variants. Each of the Gln²³⁹ → X variants (X = Ala, Asn, Glu, His, or Leu) altered the hydrogen bond potential and/or bulk of the target residue pocket, disrupting the positioning of the target residue. This incorrect positioning could have impacted any one of several steps within the kinetic mechanism, which may

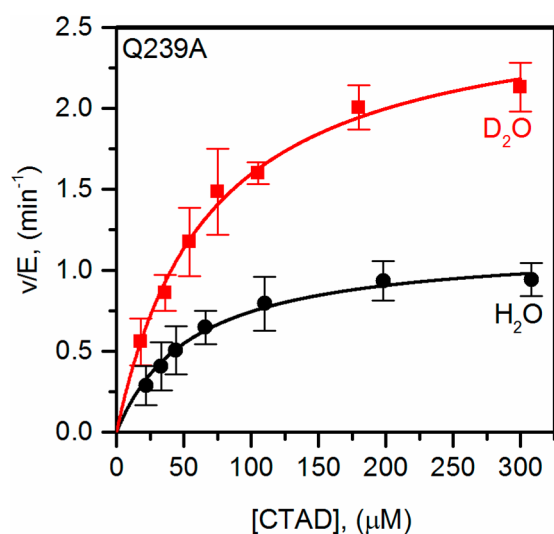


Figure 3. Steady-state kinetics of Q239A in H₂O (●) and 96% D₂O (■) buffers. FIH (1.5–30 μM), ascorbate (2 mM), αKG (500 μM), FeSO₄ (25 μM), and CTAD (0–300 μM) were in 50 mM HEPES (pH 7.00).

be distinguished through analysis of steady-state kinetic parameters and coupling ratios. The significant reduction in k_{cat} and $k_{\text{cat}}/K_{\text{M(CTAD)}}$ relative to those of WT-FIH indicated that the anchor residue played a prominent role in supporting turnover. Keeping in mind the observation that the binding affinity of CTAD was unchanged from that of WT-FIH (Table 2), we are led to conclude that the predominant role of FIH-Gln²³⁹ is to position substrate for a chemical step rather than to bind CTAD.

Although it may seem surprising that the anchor residue FIH-Gln²³⁹ contributes very little to the CTAD binding affinity, this is consistent with prior studies of CTAD variants. As the length of the CTAD has been shown to have a significant affect on the K_{M} ⁵⁶ and the binding affinity of WT-FIH for CTAD is indistinguishable from the Michaelis constant, it appears that the dominant factor in CTAD binding is the surface contact with FIH, with only minor contributions from the target residue pocket. Alanine scanning point mutagenesis of CTAD revealed that CTAD-Val⁸⁰² was the most significant residue for CTAD binding, with a 2-fold increase in the $K_{\text{M(CTAD)}}$ for the CTAD-Val⁸⁰² → Ala variant.⁵⁷ Molecular dynamics studies suggested that this mutation led to reorientation of Asn⁸⁰³, perhaps because of disruption of the tight turn conformation in residues 801–803 of CTAD. Further support for a minimal impact of FIH-Gln²³⁹ on CTAD binding is the observation that FIH hydroxylates substrates with target residues other than

asparagine.^{58,59} The structural features of these substrates suggest the overall contact between FIH and the CTAD peptide is important in determining substrate binding to FIH.^{59,60}

Inverse SKIEs and Coupling. We recently reported inverse SKIEs for WT FIH, on both k_{cat} and $k_{\text{cat}}/K_{\text{M(CTAD)}}$.²⁵ This was due to the isotopically sensitive metal–aquo fractionation prior to a rate-limiting step for WT-FIH. Importantly, WT-FIH exhibited fully coupled turnover, such that O₂ activation always led to substrate hydroxylation. Consequently, it was deduced that the rate-limiting step for k_{cat} and $k_{\text{cat}}/K_{\text{M(CTAD)}}$ was an irreversible step immediately after aquo release. This step is depicted as the oxidative decarboxylation of αKG in Scheme 1.

For each of the Gln²³⁹ → X variants, inverse SKIEs were measured on both k_{cat} and $k_{\text{cat}}/K_{\text{M(CTAD)}}$ when determined from the rate of CTAD^{OH} formation (Table 4). Although the SKIE data resembled those reported for WT-FIH, turnover for these variants was significantly uncoupled, which precluded the use of SKIEs to diagnose rate-limiting steps in the steady state. Nevertheless, uncoupling in the variants depended on solvent isotopic composition (Table 3), suggesting that the ferryl intermediate could form even when CTAD was improperly positioned. The fact that C approached unity in D₂O for these variants suggested that the main effect of the Gln²³⁹ → X change was to perturb the hydroxylation step.

Sterics and H-Bonding Impact Substrate Hydroxylation. A simple model to explain how the target residue pocket impacts productive turnover is one in which multiple conformational states of the target residue are adopted but only one conformation supports hydroxylation. X-ray crystal structures of (M+αKG)FIH bound to CTAD¹⁴ or Notch-derived peptides⁵⁵ revealed that the target residue adopted a specific rotameric conformation, with a side chain torsional angle (HN–C_α–C_β–C_γ) of –71°. This is observed for both Notch target residues Notch-Asn²¹⁰ and Notch-Asn¹⁹⁴⁵ [Protein Data Bank (PDB) entries 3P3P and 3P3N, respectively]. As a good deal of flexibility near Gln²³⁹ was observed crystallographically for (Fe+αKG)FIH when CTAD was absent (PDB entry 1MZF),⁴⁸ changing the hydrogen bonding potential and packing density of this anchor residue should alter the target residue position above the Fe(II). The significant reduction in catalytic efficiency for each point mutant strongly suggests that the major role of FIH-Gln²³⁹ is to stabilize the proper rotamer of CTAD-Asn⁸⁰³ that can undergo hydroxylation during turnover.

The kinetic data further suggest that packing near the target residue may also impact O₂ activation in FIH. The overall trend in the kinetic parameters measured by coupled turnover (Table 2) was dominated by bulk, as the kinetic parameters for the

Table 4. Apparent Kinetic Parameters in D₂O and SKIEs for FIH and Its Variants^a

	k_{cat} (min ⁻¹) ^b	$k_{\text{cat}}/K_{\text{M(CTAD)}}$ (μM ⁻¹ min ⁻¹) ^b	D ₂ O k_{cat} ^c	D ₂ O $k_{\text{cat}}/K_{\text{M(CTAD)}}$ ^d
WT ^e	59 ± 2	1.09 ± 0.11	0.51 ± 0.07	0.40 ± 0.07
Q239A	2.55 ± 0.21	0.044 ± 0.011	0.50 ± 0.05	0.48 ± 0.15
Q239N	0.27 ± 0.02	0.005 ± 0.001	0.50 ± 0.06	0.41 ± 0.18
Q239H	0.050 ± 0.003	2.0 × 10 ⁻³ ± 8 × 10 ⁻⁴	0.46 ± 0.07	0.17 ± 0.06
Q239E	0.046 ± 0.002	(8 ± 3) × 10 ⁻⁴	0.52 ± 0.05	0.41 ± 0.16
Q239L	ND ^f	ND ^f	ND ^f	ND ^f

^aIn 50 mM HEPES (pH 7.00) at 37.0 °C. ^bDetermined from assays with CTAD as the varied substrate, in ascorbate (2 mM), αKG (500 μM), FeSO₄ (25 μM), and CTAD (0–250 μM); $\chi_{\text{D}_2\text{O}} = 0.96$. ^c ${}^{\text{D}_2\text{O}}k_{\text{cat}} = k_{\text{cat}(\text{H}_2\text{O})}/k_{\text{cat}(\text{D}_2\text{O})}$. ^d ${}^{\text{D}_2\text{O}}k_{\text{cat}}/K_{\text{M(CTAD)}} = [k_{\text{cat}}/K_{\text{M(CTAD)}}]_{\text{in H}_2\text{O}}/[k_{\text{cat}}/K_{\text{M(CTAD)}}]_{\text{in D}_2\text{O}}$. ^eFrom ref 25. ^fNot determined.

Gln²³⁹ → X point variants decreased monotonically in a series: X = (Ala > Asn > Glu and His ≫ Leu). As the kinetic parameters of the variants listed in Table 2 are functions of all steps leading to CTAD hydroxylation, it is not possible to separately identify the impact of the variants on O₂ activation. However, the coupling data directly measured succinate production (Table 4), which reports directly on O₂ activation. The rates of succinate production clearly showed that each variant produced succinate much more slowly than WT-FIH, suggesting that O₂ activation was slowed in these variants. As the packing about CTAD-Asn⁸⁰³ is quite tight in WT-FIH,¹⁴ it is possible that the Gln²³⁹ → X variants excluded CTAD-Asn⁸⁰³ from the proper conformation, which could impede access of O₂ to the Fe(II) as well as hydroxylation by the putative ferryl intermediate (Scheme 2).

CONCLUSION

This work establishes that proper positioning of the primary substrate (CTAD) is required to support coupled turnover by FIH. We conclude that proper positioning of substrate is crucial for the hydroxylation of CTAD as well as for stimulation of O₂ activation. Mispositioned CTAD impedes O₂ activation, suggesting that the environment near the Fe(II) cofactor plays a marked role in O₂ activation.

ASSOCIATED CONTENT

Supporting Information

Control experiments showing the thermal stability of the Gln²³⁹ → X variant and intrinsic tryptophan fluorescence titrations with CTAD. This material is available free of charge via the Internet at <http://pubs.acs.org>.

AUTHOR INFORMATION

Corresponding Author

*Department of Chemistry, University of Massachusetts, Amherst, MA 01003. E-mail: mknapp@chem.umass.edu. Phone: (413) 545-4001. Fax: (413) 545-4490.

Funding

Research reported in this publication was supported by National Institutes of Health Grant R01-GM077413 and National Institutes of Health Chemistry-Biology Interface Predoctoral Training Fellowship T32-GM008515.

Notes

The authors declare no competing financial interest.

ACKNOWLEDGMENTS

We thank Dr. Evren Saban for the purification of the Gln²³⁹ → Asn variant and the late Professor Robert Weiss for the use of his differential scanning calorimeter.

ABBREVIATIONS

αKG, α-ketoglutarate; CAS, clavamate synthase; CD, circular dichroism; CREBP, cAMP response element-binding protein; CTAD, C-terminal transactivation domain; DFT, density functional theory; DTT, dithiothreitol; FIH, factor-inhibiting HIF; HAT, hydrogen atom transfer; HEPES, 4-(2-hydroxyethyl)-1-piperazineethanesulfonic acid; HIF, hypoxia inducible factor-1α; MCD, magnetic circular dichroism; NOG, N-oxalyl glycine; P4H, prolyl-4-hydroxylase; SKIE, solvent kinetic isotope effect; TauD, taurine dioxygenase.

REFERENCES

- (1) Hausinger, R. P. (2004) Fe(II)/α-Ketoglutarate-dependent hydroxylases and related enzymes. *Crit. Rev. Biochem. Mol. Biol.* 39, 21–68.
- (2) Purpero, V., and Moran, G. R. (2007) The diverse and pervasive chemistries of the α-keto acid dependent enzymes. *JBIC, J. Biol. Inorg. Chem.* 12, 587–601.
- (3) Jaakkola, P., Mole, D. R., Tian, Y. M., Wilson, M. I., Gielbert, J., Gaskell, S. J., von Kriegsheim, A., Hebestreit, H. F., Mukherji, M., Schofield, C. J., Maxwell, P. H., Pugh, C. W., and Ratcliffe, P. J. (2001) Targeting of HIF-α to the von Hippel-Lindau ubiquitylation complex by O₂-regulated prolyl hydroxylation. *Science* 292, 468–472.
- (4) Lando, D., Peet, D. J., Whelan, D. A., Gorman, J. J., and Whitelaw, M. L. (2002) Asparagine hydroxylation of the HIF transactivation domain a hypoxic switch. *Science* 295, 858–861.
- (5) Duncan, T., Treweek, S. C., Koivisto, P., Bates, P. A., Lindahl, T., and Sedgwick, B. (2002) Reversal of DNA alkylation damage by two human dioxygenases. *Proc. Natl. Acad. Sci. U.S.A.* 99, 16660–16665.
- (6) Treweek, S. C., Henshaw, T. F., Hausinger, R. P., Lindahl, T., and Sedgwick, B. (2002) Oxidative demethylation by *Escherichia coli* AlkB directly reverts DNA base damage. *Nature* 419, 174–178.
- (7) Tsukada, Y., Fang, J., Erdjument-Bromage, H., Warren, M. E., Borchers, C. H., Tempst, P., and Zhang, Y. (2006) Histone demethylation by a family of JmjC domain-containing proteins. *Nature* 439, 811–816.
- (8) Zheng, G., Dahl, J. A., Niu, Y., Fedorcsak, P., Huang, C.-M., Li, C. J., Vagbo, C. B., Shi, Y., Wang, W.-L., Song, S.-H., Lu, Z., Bosmans, R. P. G., Dai, Q., Hao, Y.-J., Yang, X., Zhao, W.-M., Tong, W.-M., Wang, X.-J., Bogdan, F., Furu, K., Fu, Y., Jia, G., Zhao, X., Liu, J., Krokan, H. E., Klungland, A., Yang, Y.-G., and He, C. (2013) ALKBH5 Is a Mammalian RNA Demethylase that Impacts RNA Metabolism and Mouse Fertility. *Mol. Cell* 49, 18–29.
- (9) Jia, G., Fu, Y., Zhao, X., Dai, Q., Zheng, G., Yang, Y., Yi, C., Lindahl, T., Pan, T., Yang, Y.-G., and He, C. (2011) N⁶-Methyladenosine in nuclear RNA is a major substrate of the obesity-associated FTO. *Nat. Chem. Biol.* 7, 885–887.
- (10) Rose, N. R., McDonough, M. A., King, O. N. F., Kawamura, A., and Schofield, C. J. (2011) Inhibition of 2-oxoglutarate dependent oxygenases. *Chem. Soc. Rev.* 40, 4364–4397.
- (11) Loenarz, C., and Schofield, C. J. (2011) Physiological and biochemical aspects of hydroxylations and demethylations catalyzed by human 2-oxoglutarate oxygenases. *Trends Biochem. Sci.* 36, 7–18.
- (12) Holme, E. (1975) Kinetic study of thymine 7-hydroxylase from *Neurospora crassa*. *Biochemistry* 14, 4999–5003.
- (13) De Carolis, E., and De Luca, V. (1993) Purification, characterization, and kinetic analysis of a 2-oxoglutarate-dependent dioxygenase involved in vindoline biosynthesis from *Catharanthus roseus*. *J. Biol. Chem.* 268, 5504–5511.
- (14) Elkins, J. M., Hewitson, K. S., McNeill, L. A., Seibel, J. F., Schlemminger, I., Pugh, C. W., Ratcliffe, P. J., and Schofield, C. J. (2003) Structure of factor-inhibiting hypoxia-inducible factor (HIF) reveals mechanism of oxidative modification of HIF-1α. *J. Biol. Chem.* 278, 1802–1806.
- (15) Ozer, A., and Bruick, R. K. (2007) Non-heme dioxygenases: Cellular sensors and regulators jelly rolled into one? *Nat. Chem. Biol.* 3, 144–153.
- (16) Semenza, G. L. (2004) Hydroxylation of HIF-1: Oxygen sensing at the molecular level. *Physiology* 19, 176–182.
- (17) Iyer, N. V., Kotch, L. E., Agani, F., Leung, S. W., Laughner, E., Wenger, R. H., Gassmann, M., Gearhart, J. D., Lawler, A. M., Yu, A. Y., and Semenza, G. L. (1998) Cellular and developmental control of O₂ homeostasis by hypoxia-inducible factor 1α. *Genes Dev.* 12, 149–162.
- (18) Semenza, G. L. (2003) Targeting HIF-1 for cancer therapy. *Nat. Rev. Cancer* 3, 721–32.
- (19) Metzzen, E., and Ratcliffe, P. J. (2004) HIF hydroxylation and cellular oxygen sensing. *Biol. Chem.* 385, 223–230.
- (20) McNeill, L. A., Hewitson, K. S., Claridge, T. D., Seibel, J. F., Horsfall, L. E., and Schofield, C. J. (2002) Hypoxia-inducible factor

asparaginyl hydroxylase (FIH-1) catalyses hydroxylation at the β -carbon of asparagine-803. *Biochem. J.* 367, 571–575.

(21) Lando, D., Peet, D. J., Gorman, J. J., Whelan, D. A., Whitelaw, M. L., and Bruick, R. K. (2002) FIH-1 is an asparaginyl hydroxylase enzyme that regulates the transcriptional activity of hypoxia-inducible factor. *Genes Dev.* 16, 1466–1471.

(22) Price, J. C., Barr, E. W., Hoffart, L. M., Krebs, C., and Bollinger, J. M. (2005) Kinetic dissection of the catalytic mechanism of taurine: α -ketoglutarate dioxygenase (TauD) from *Escherichia coli*. *Biochemistry* 44, 8138–8147.

(23) Salowe, S. P., Marsh, E. N., and Townsend, C. A. (1990) Purification and characterization of clavamate synthase from *Streptomyces clavuligerus*: An unusual oxidative enzyme in natural product biosynthesis. *Biochemistry* 29, 6499–6508.

(24) Thornburg, L. D., Lai, M. T., Wishnok, J. S., and Stubbe, J. (1993) A non-heme iron protein with heme tendencies: An investigation of the substrate specificity of thymine hydroxylase. *Biochemistry* 32, 14023–14033.

(25) Hangasky, J. A., Saban, E., and Knapp, M. J. (2013) Inverse Solvent Isotope Effects Arising from Substrate Triggering in the Factor Inhibiting Hypoxia Inducible Factor. *Biochemistry* 52, 1594–1602.

(26) Zhou, J., Kelly, W. L., Bachmann, B. O., Gunsior, M., Townsend, C. A., and Solomon, E. I. (2001) Spectroscopic studies of substrate interactions with clavamate synthase 2, a multifunctional α -KG-dependent non-heme iron enzyme: Correlation with mechanisms and reactivities. *J. Am. Chem. Soc.* 123, 7388–7398.

(27) Zhou, J., Gunsior, M., Bachmann, B. O., Townsend, C. A., and Solomon, E. I. (1998) Substrate Binding to the α -Ketoglutarate-Dependent Non-Heme Iron Enzyme Clavamate Synthase 2: Coupling Mechanism of Oxidative Decarboxylation and Hydroxylation. *J. Am. Chem. Soc.* 120, 13539–13540.

(28) Pavel, E. G., Zhou, J., Busby, R. W., Gunsior, M., Townsend, C. A., and Solomon, E. I. (1998) Circular dichroism and magnetic circular dichroism spectroscopic studies of the non-heme ferrous active site in clavamate synthase and its interaction with α -ketoglutarate cosubstrate. *J. Am. Chem. Soc.* 120, 743–753.

(29) Whiting, A. K., Que, L., Saari, R. E., Hausinger, R. P., Fredrick, M. A., and McCracken, J. (1997) Metal Coordination Environment of a Cu(II)-Substituted α -Keto Acid-Dependent Dioxygenase That Degrades the Herbicide 2,4-D. *J. Am. Chem. Soc.* 119, 3413–3414.

(30) Light, K. M., Hangasky, J. A., Knapp, M. J., and Solomon, E. I. (2013) Spectroscopic Studies of the Mononuclear Non-Heme Fe-II Enzyme FIH: Second-Sphere Contributions to Reactivity. *J. Am. Chem. Soc.* 135, 9665–9674.

(31) Neidig, M. L., Brown, C. D., Light, K. M., Fujimori, D. G., Nolan, E. M., Price, J. C., Barr, E. W., Bollinger, J. M., Krebs, C., Walsh, C. T., and Solomon, E. I. (2007) CD and MCD of CytC3 and taurine dioxygenase: Role of the facial triad in α -KG-dependent oxygenases. *J. Am. Chem. Soc.* 129, 14224–14231.

(32) Price, J. C., Barr, E. W., Tirupati, B., Bollinger, J. M., and Krebs, C. (2003) The First Direct Characterization of a High-Valent Iron Intermediate in the Reaction of an α -Ketoglutarate-Dependent Dioxygenase: A High-Spin Fe(IV) Complex in Taurine/ α -Ketoglutarate Dioxygenase (TauD) from *Escherichia coli*. *Biochemistry* 42, 7497–7508.

(33) Riggs-Gelasco, P. J., Price, J. C., Guyer, R. B., Brehm, J. H., Barr, E. W., Bollinger, J. M., and Krebs, C. (2004) EXAFS spectroscopic evidence for an Fe=O unit in the Fe(IV) intermediate observed during oxygen activation by taurine: α -ketoglutarate dioxygenase. *J. Am. Chem. Soc.* 126, 8108–8109.

(34) Proshlyakov, D. A., Henshaw, T. F., Monterosso, G. R., Ryle, M. J., and Hausinger, R. P. (2004) Direct detection of oxygen intermediates in the non-heme Fe enzyme taurine/ α -ketoglutarate dioxygenase. *J. Am. Chem. Soc.* 126, 1022–1023.

(35) Hoffart, L. M., Barr, E. W., Guyer, R. B., Bollinger, J. M., and Krebs, C. (2006) Direct spectroscopic detection of a C-H-cleaving high-spin Fe(IV) complex in a prolyl-4-hydroxylase. *Proc. Natl. Acad. Sci. U.S.A.* 103, 14738–14743.

(36) Price, J. C., Barr, E. W., Glass, T. E., Krebs, C., and Bollinger, J. M. (2003) Evidence for Hydrogen Abstraction from C1 of Taurine by the High-Spin Fe(IV) Intermediate Detected during Oxygen Activation by Taurine: α -Ketoglutarate Dioxygenase (TauD). *J. Am. Chem. Soc.* 125, 13008–13009.

(37) Ryle, M. J., Liu, A., Muthukumar, R. B., Ho, R. Y. N., Koehntop, K. D., McCracken, J., Que, L., and Hausinger, R. P. (2003) O₂- and α -Ketoglutarate-Dependent Tyrosyl Radical Formation in TauD, an α -Keto Acid-Dependent Non-Heme Iron Dioxygenase. *Biochemistry* 42, 1854–1862.

(38) Saban, E., Flagg, S., and Knapp, M. (2011) Uncoupled O₂-activation in the human HIF-asparaginyl hydroxylase, FIH, does not produce reactive oxygen species. *JBIC, J. Biol. Inorg. Chem.* 105, 630–636.

(39) Solomon, E. I., Brunold, T. C., Davis, M. I., Kemsley, J. N., Lee, S.-K., Lehnert, N., Neese, F., Skulan, A. J., Yang, Y.-S., and Zhou, J. (2000) Geometric and Electronic Structure/Function Correlations in Non-Heme Iron Enzymes. *Chem. Rev.* 100, 235–350.

(40) Saban, E., Chen, Y.-H., Hangasky, J., Taabazuing, C., Holmes, B., and Knapp, M. (2011) The second coordination sphere of FIH controls hydroxylation. *Biochemistry* 50, 4733–4740.

(41) Borowski, T., Bassan, A., and Siegbahn, P. E. M. (2004) Mechanism of dioxygen activation in 2-oxoglutarate-dependent enzymes: A hybrid DFT study. *Chem.—Eur. J.* 10, 1031–1041.

(42) De Visser, S. P. (2007) Can the peroxosuccinate complex in the catalytic cycle of taurine/ α -ketoglutarate dioxygenase (TauD) act as an alternative oxidant? *Chem. Commun.* 171–173.

(43) Diebold, A. R., Brown-Marshall, C. D., Neidig, M. L., Brownlee, J. M., Moran, G. R., and Solomon, E. I. (2011) Activation of α -Keto Acid-Dependent Dioxygenases: Application of an {FeNO}₇/{FeO₂}₈ Methodology for Characterizing the Initial Steps of O₂ Activation. *J. Am. Chem. Soc.* 133, 18148–18160.

(44) Ye, S., Riplinger, C., Hansen, A., Krebs, C., Bollinger, J. M., and Neese, F. (2012) Electronic Structure Analysis of the Oxygen-Activation Mechanism by FeII- and α -Ketoglutarate (α KG)-Dependent Dioxygenases. *Chem.—Eur. J.* 18, 6555–6567.

(45) Mirica, L. M., McCusker, K. P., Munos, J. W., Liu, H., and Klinman, J. P. (2008) ¹⁸O kinetic isotope effects in non-heme iron enzymes: Probing the nature of Fe/O₂ intermediates. *J. Am. Chem. Soc.* 130, 8122–8123.

(46) Ryle, M. J., Padmakumar, R., and Hausinger, R. P. (1999) Stopped-Flow Kinetic Analysis of *Escherichia coli* Taurine/ α -Ketoglutarate Dioxygenase: Interactions with α -Ketoglutarate, Taurine, and Oxygen. *Biochemistry* 38, 15278–15286.

(47) Flashman, E., Hoffart, L. M., Hamed, R. B., Bollinger, J. M., Krebs, C., and Schofield, C. J. (2010) Evidence for the slow reaction of hypoxia-inducible factor prolyl hydroxylase 2 with oxygen. *FEBS J.* 277, 4089–4099.

(48) Dann, C. E., Bruick, R. K., and Deisenhofer, J. (2002) Structure of factor-inhibiting hypoxia-inducible factor 1: An asparaginyl hydroxylase involved in the hypoxic response pathway. *Proc. Natl. Acad. Sci. U.S.A.* 99, 15351–15356.

(49) Lee, C., Kim, S. J., Jeong, D. G., Lee, S. M., and Ryu, S. E. (2003) Structure of Human FIH-1 Reveals a Unique Active Site Pocket and Interaction Sites for HIF-1 and von Hippel-Lindau. *J. Biol. Chem.* 278, 7558–7563.

(50) Chen, Y. H., Comeaux, L. M., Herbst, R. W., Saban, E., Kennedy, D. C., Maroney, M. J., and Knapp, M. J. (2008) Coordination changes and auto-hydroxylation of FIH-1: Uncoupled O₂-activation in a human hypoxia sensor. *J. Inorg. Biochem.* 102, 2120–2129.

(51) Frantom, P. A., and Fitzpatrick, P. F. (2003) Uncoupled forms of tyrosine hydroxylase unmask kinetic isotope effects on chemical steps. *J. Am. Chem. Soc.* 125, 16190–16191.

(52) Loeb, K. E., Westre, T. E., Kappock, T. J., Mitic, N., Glasfeld, E., Caradonna, J. P., Hedman, B., Hodgson, K. O., and Solomon, E. I. (1997) Spectroscopic characterization of the catalytically competent ferrous site of the resting, activated, and substrate-bound forms of phenylalanine hydroxylase. *J. Am. Chem. Soc.* 119, 1901–1915.

(53) Hegg Whiting, A. K., Saari, R. E., McCracken, J., Hausinger, R. P., and Que, L., Jr. (1999) Herbicide degrading α -keto acid dependent enzyme TfdA: Metal coordination environment and mechanistic insights. *Biochemistry* 38, 16714–16726.

(54) Bollinger, J. M., Price, J. C., Hoffart, L. M., Barr, E. W., and Krebs, C. (2005) Mechanism of Taurine: α -Ketoglutarate Dioxygenase (TauD) from *Escherichia coli*. *Eur. J. Inorg. Chem.* 2005, 4245–4254.

(55) Coleman, M. L., McDonough, M. A., Hewitson, K. S., Coles, C., Mecinović, J., Edelmann, M., Cook, K. M., Cockman, M. E., Lancaster, D. E., Kessler, B. M., Oldham, N. J., Ratcliffe, P. J., and Schofield, C. J. (2007) Asparaginyl Hydroxylation of the Notch Ankyrin Repeat Domain by Factor Inhibiting Hypoxia-inducible Factor. *J. Biol. Chem.* 282, 24027–24038.

(56) Koivunen, P., Hirsilä, M., Günzler, V., Kivirikko, K. I., and Myllyharju, J. (2004) Catalytic properties of the asparaginyl hydroxylase (FIH) in the oxygen sensing pathway are distinct from those of its prolyl 4-hydroxylases. *J. Biol. Chem.* 279, 9899–9904.

(57) Linke, S., Stojkoski, C., Kewley, R. J., Booker, G. W., Whitelaw, M. L., and Peet, D. J. (2004) Substrate requirements of the oxygen-sensing asparaginyl hydroxylase factor-inhibiting hypoxia-inducible factor. *J. Biol. Chem.* 279, 14391–14397.

(58) Yang, M., Chowdhury, R., Ge, W., Hamed, R. B., McDonough, M. A., Claridge, T. D. W., Kessler, B. M., Cockman, M. E., Ratcliffe, P. J., and Schofield, C. J. (2011) Factor-inhibiting hypoxia-inducible factor (FIH) catalyses the post-translational hydroxylation of histidinyl residues within ankyrin repeat domains. *FEBS J.* 278, 1086–1097.

(59) Yang, M., Hardy, A. P., Chowdhury, R., Loik, N. D., Scotti, J. S., McCullagh, J. S. O., Claridge, T. D. W., McDonough, M. A., Ge, W., and Schofield, C. J. (2013) Substrate Selectivity Analyses of Factor Inhibiting Hypoxia-Inducible Factor. *Angew. Chem., Int. Ed.* 52, 1700–1704.

(60) Wilkins, S. E., Karttunen, S., Hampton-Smith, R. J., Murchland, I., Chapman-Smith, A., and Peet, D. J. (2012) Factor Inhibiting HIF (FIH) Recognizes Distinct Molecular Features within Hypoxia-inducible Factor- α (HIF- α) versus Ankyrin Repeat Substrates. *J. Biol. Chem.* 287, 8769–8781.